

## LA-UR-18-28892

Approved for public release; distribution is unlimited.

Title: Assessment of Hydriding in the U-Si System

Author(s): Shivprasad, Aditya Prahlad  
Wermer, Joseph Raymond  
White, Joshua Taylor

Intended for: Report

Issued: 2019-07-23 (rev.2)

---

**Disclaimer:**

Los Alamos National Laboratory, an affirmative action/equal opportunity employer, is operated by Triad National Security, LLC for the National Nuclear Security Administration of U.S. Department of Energy under contract 89233218CNA000001. By approving this article, the publisher recognizes that the U.S. Government retains nonexclusive, royalty-free license to publish or reproduce the published form of this contribution, or to allow others to do so, for U.S. Government purposes. Los Alamos National Laboratory requests that the publisher identify this article as work performed under the auspices of the U.S. Department of Energy. Los Alamos National Laboratory strongly supports academic freedom and a researcher's right to publish; as an institution, however, the Laboratory does not endorse the viewpoint of a publication or guarantee its technical correctness.

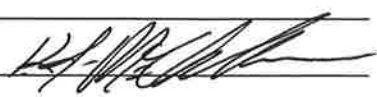
## APPENDIX E

### NTRD DOCUMENT COVER SHEET<sup>1</sup>

Name/Title of Deliverable/Milestone/Revision No. M3NT-18LA020201026; Assessment of hydriding in the U-Si system

Work Package Title and Number NT-18LA02020102; Advanced Ceramic Fuel Development - LANL

Work Package WBS Number 1.02.02.02.01 - LWR Fuels

Responsible Work Package Manager Ken McClellan   
(Name/Signature)

Date Submitted **September 21, 2018**

Quality Rigor Level for Deliverable/Milestone <sup>2</sup>	<input type="checkbox"/> QRL-1 <input type="checkbox"/> Nuclear Data	<input type="checkbox"/> QRL-2	<input checked="" type="checkbox"/> QRL-3	<input type="checkbox"/> QRL 4 Lab QA Program <sup>3</sup>
--	---	--------------------------------	---	---

This deliverable was prepared in accordance with Los Alamos National Laboratory  
(Participant/National Laboratory Name)

QA program which meets the requirements of  
☒ DOE Order 414.1 ☐ NQA-1 ☐ Other

**This Deliverable was subjected to:**

☐ Technical Review

**Technical Review (TR)**

**Review Documentation Provided**

- ☐ Signed TR Report or,  
☐ Signed TR Concurrence Sheet or,  
☒ Signature of TR Reviewer(s) below

**Name and Signature of Reviewers**

NICHOLAS Digitally signed by NICHOLAS  
WOZNIAK (Affiliate) WOZNIAK (Affiliate)  
Date: 2018.09.19 15:51:09 -06'00'

☐ Peer Review

**Peer Review (PR)**

**Review Documentation Provided**

- ☐ Signed PR Report or,  
☐ Signed PR Concurrence Sheet or,  
☐ Signature of PR Reviewer(s) below

**Name and Signature of Reviewers**

**NOTE 1:** Appendix E should be filled out and submitted with each deliverable. Or, if the PICS: NE system permits, completely enter all applicable information in the PICS: NE Deliverable Form. The requirement is to ensure that all applicable information is entered either in the PICS: NE system or by using the NTRD Document Cover Sheet.

- In some cases there may be a milestone where an item is being fabricated, maintenance is being performed on a facility, or a document is being issued through a formal document control process where it specifically calls out a formal review of the document. In these cases, documentation (e.g., inspection report, maintenance request, work planning package documentation or the documented review of the issued document through the document control process) of the completion of the activity, along with the Document Cover Sheet, is sufficient to demonstrate achieving the milestone.

**NOTE 2:** If QRL 1, 2, or 3 is not assigned, then the QRL 4 box must be checked, and the work is understood to be performed using laboratory QA requirements. This includes any deliverable developed in conformance with the respective National Laboratory / Participant, DOE or NNSA-approved QA Program.

**NOTE 3:** If the lab has an NQA-1 program and the work to be conducted requires an NQA-1 program, then the QRL-1 box must be checked in the work Package and on the Appendix E cover sheet and the work must be performed in accordance with the Lab's NQA-1 program. The QRL-4 box should not be checked.

# ***Assessment of Hydridding in the U-Si System***

**Nuclear Technology  
Research and Development**

***Prepared for  
U.S. Department of Energy  
FCRD Program***

***Aditya P. Shivprasad***

***Joseph R. Wermer***

***Joshua T. White***

***Los Alamos National Laboratory***

***September 21, 2018***

**NTRD- M3NT-18LA020201026**

**LA-UR-18-28892**





#### **DISCLAIMER**

This information was prepared as an account of work sponsored by an agency of the U.S. Government. Neither the U.S. Government nor any agency thereof, nor any of their employees, makes any warranty, expressed or implied, or assumes any legal liability or responsibility for the accuracy, completeness, or usefulness, of any information, apparatus, product, or process disclosed, or represents that its use would not infringe privately owned rights. References herein to any specific commercial product, process, or service by trade name, trade mark, manufacturer, or otherwise, does not necessarily constitute or imply its endorsement, recommendation, or favoring by the U.S. Government or any agency thereof. The views and opinions of authors expressed herein do not necessarily state or reflect those of the U.S. Government or any agency thereof.



## **SUMMARY**

Fuels with high uranium densities have been considered in the Nuclear Technology Research and Development program's Advanced Fuels Campaign as potential replacements for uranium(IV) oxide in commercial light water reactors. One such candidate fuel is  $\text{U}_3\text{Si}_2$ , which has been observed to readily oxidize and potentially hydride in steam and simulated pressurized water reactor conditions. The hydrogen absorption properties of  $\text{U}_3\text{Si}_2$ , in particular, are not well-understood.

Research this FY has focused on developing a better understanding of the hydrogen absorption characteristics of  $\text{U}_3\text{Si}_2$  in steam and in pure hydrogen. Pellets of  $\text{U}_3\text{Si}_2$  were exposed to 75% steam at various temperatures and monitored for mass changes using thermogravimetric analysis, while pellets and ingots exposed to pure hydrogen in a Sieverts' apparatus exhibited signs of hydrogen absorption. It was observed that hydrogen absorption of  $\text{U}_3\text{Si}_2$  required higher pressures of hydrogen than those required to hydride uranium metal at similar temperatures.





## CONTENTS

SUMMARY .....	iii
ACRONYMS .....	vii
1. INTRODUCTION .....	1
2. Experimental methods.....	5
2.1 Materials.....	5
2.2 Steam corrosion testing.....	5
2.3 Sieverts' gas absorption .....	6
2.4 Microstructural analysis.....	7
3. Results and discussion.....	8
3.1 Steam corrosion testing.....	8
3.2 Sieverts' gas absorption .....	13
3.3 Microstructural analysis.....	15
4. Summary and future work.....	15
5. Bibliography.....	17

## FIGURES

Figure 1: Isothermal exposures of $U_3Si_2$ pellets to flowing 6% $H_2/Ar$ at 350 (magenta), 375 (blue), and 400 (red) °C. Isothermal data for $U_3Si_2$ in flowing steam at 400 °C is shown in black for comparison. Figure and caption adapted from (Wood et al., 2018).....	2
Figure 2: Weight change measured for $U_3Si_2$ samples as a function of exposure time at 300 °C for two different water chemistry conditions. Error bars represent average of multiple samples and standard error of measurement technique. A trend line is added to the 1-ppm $H_2$ sample data to guide the eye. Samples tested at 6-ppm $H_2$ fully pulverized when examined after 38 days so measurement was not possible. Figure and caption adapted from (Nelson et al., 2018).....	3
Figure 3: Micrograph taken from a cross-sectioned $U_3Si_2$ pellet exposed to steam at 400 °C. Pellet was exposed for 1.5-hr. Unknown phase is hypothesized to be hydride-phase lamellae. Figure and caption adapted from (Wood et al., 2018).....	4
Figure 4: Experimental setup for steam TGA analysis. Annotations indicate major components of the system. ....	6
Figure 5: Experimental apparatus for Sieverts' gas absorption. Important components of the apparatus are annotated. ....	7
Figure 6: Mass gain for $U_3Si_2$ exposed to 75% steam at 250 °C for 10-hr. Data is smoothed using a moving average filter with moving average span of 5. In the inset is an image of the sample post-testing.....	8
Figure 7: Mass gain for $U_3Si_2$ exposed to 75% steam at 300 °C for 10-hr. Data is smoothed using a moving average filter with moving average span of 5. In the inset is an image of the sample post-testing.....	9
Figure 8: Mass gain for $U_3Si_2$ exposed to 75% steam at 350 °C for 10-hr. Data is smoothed using a moving average filter with moving average span of 5. In the inset is an image of the sample post-testing.....	10
Figure 9: Mass gain for $U_3Si_2$ exposed to 75% steam at 500 °C for 10-hr. Data is smoothed using a moving average filter with moving average span of 5. In the inset is an image of the sample post-testing.....	11
Figure 10: $U_3Si_2$ exposed to 75% steam at 700 °C. Corrosion test lasted only a few seconds before the temperature spike due to oxidation caused a soft reset of the instrument.....	12
Figure 11: Comparison between mass gains at 250 (blue), 300 (orange), 350 (yellow) °C in 75% steam. Data is smoothed to show general trends in mass change, only, and is not considered analytical. ....	12
Figure 12: Comparison between mass gains at 250 (blue), 300 (orange), 350 (yellow), and 500 (purple) °C in 75% steam. Data is smoothed using a moving average filter with moving average span of 5.....	13
Figure 13: Preliminary pressure-composition-isotherm for $U_3Si_2$ in hydrogen at 350 °C. ....	14
Figure 14: XRD pattern collected from $U_3Si_2$ exposed to hydrogen gas at 860 torr and 400 °C. Data from this study is shown in blue, while data from exposure of $U_3Si_2$ to flowing 6% $H_2/Ar$ at 355 °C for 50-hr from (Wood et al., 2018). Red bars indicate the PDF peak indices for $U_3Si_2$ , while blue bars indicate peak indices for $U_3Si_2H_{1.8}$ from (Mašková et al., 2017, p. 2). ....	15

## **ACRONYMS**

PWR	Pressurized water reactor
FRL	Fuels Research Laboratory
XRD	X-ray diffraction
TGA	Thermogravimetric analysis/analyzer
H/U	Hydrogen-to-uranium ratio
PCT	Pressure-composition-temperature
PDF	Powder diffraction file



# ASSESSMENT OF HYDRIDING IN THE U-SI SYSTEM

## 1. INTRODUCTION

Uranium silicides, such as  $\text{U}_3\text{Si}_2$ , are promising candidates for accident tolerant fuels because of their high thermal conductivities and uranium densities, as compared with  $\text{UO}_2$ . Higher thermal conductivity results in lower fuel centerline temperatures during operation and, thus, lower stored energy of the reactor core. Additionally, thermal conductivities of these compounds increase with temperature, which will help mitigate fuel rod damage during a reactivity-initiated accident such as a control rod ejection or a large break loss of coolant accident.

High uranium density results in an increased fission density and, thus, allows for a greater neutronic penalty from accident tolerant fuel claddings. Proposed accident tolerant claddings include stainless steel, Fe-Cr-Al (and derivative alloys), and silicon carbide because of their improved resistance to waterside corrosion compared to zirconium-based fuel cladding. However, all of these cladding concepts use elements with higher neutron absorption cross-sections than zirconium. Because of this, the improved fission density of uranium silicides enables the use of these types of cladding in reactors.

In addition to accident tolerance with respect to neutronics and thermal conductivity, it is important to assess the behavior of  $\text{U}_3\text{Si}_2$  in a cladding breach scenario. However, resistance of uranium silicides to waterside corrosion during such conditions is not well-understood. In particular,  $\text{U}_3\text{Si}_2$  exposed to high-temperature steam and simulated pressurized water reactor (PWR) environments has been observed to degrade by rapid pulverization.

Previous work in FY17 within the campaign examined the performance of  $\text{U}_3\text{Si}_2$  in a variety of environments such as synthetic air (21%  $\text{O}_2$ , balance Ar), 75% steam, high-temperature/pressure water with hydrogen water chemistry, and 6%  $\text{H}_2$ /Ar (Wood et al., 2018; Nelson et al., 2018). These tests were carried out *in-situ* using thermogravimetric analysis in the cases of synthetic air, steam, and hydrogen and in-autoclave for simulated PWR conditions.

Thermogravimetric analysis in steam and 6%  $\text{H}_2$ /Ar (Figure 1), as well as simulated PWR conditions (Figure 2), showed significant mass loss. For waterside corrosion, mass loss occurred over days, while in steam and hydrogen environments, mass loss occurred over the course of minutes to hours. Microstructural analysis of samples tested in these conditions showed evidence of an unidentified secondary phase and comparison with literature lead to the hypothesis that  $\text{U}_3\text{Si}_2$  absorbs hydrogen to form a hydride phase that spalls off and exposes the corrosion medium to new surfaces. An example of the observed secondary phase in a steam-corroded samples is shown in Figure 3. The existence of a hydride phase was further supported by the calculation of a  $\text{U}_3\text{Si}_2\text{H}_{2-x}$  phase using density functional theory (DFT) methods (Mašková et al., 2017, p. 2; Middleburgh et al., 2018). The hydride phase studied in literature was formed at very high pressures of hydrogen (12 MPa) and varying temperature (between 25 and 500 °C during a temperature ramp and cooling) (Mašková et al., 2017, p. 2). Because the hydrides were formed under variable conditions, the hydrogen content of this phase and the conditions for producing it are not well-understood, especially as a function of temperature and hydrogen pressure.

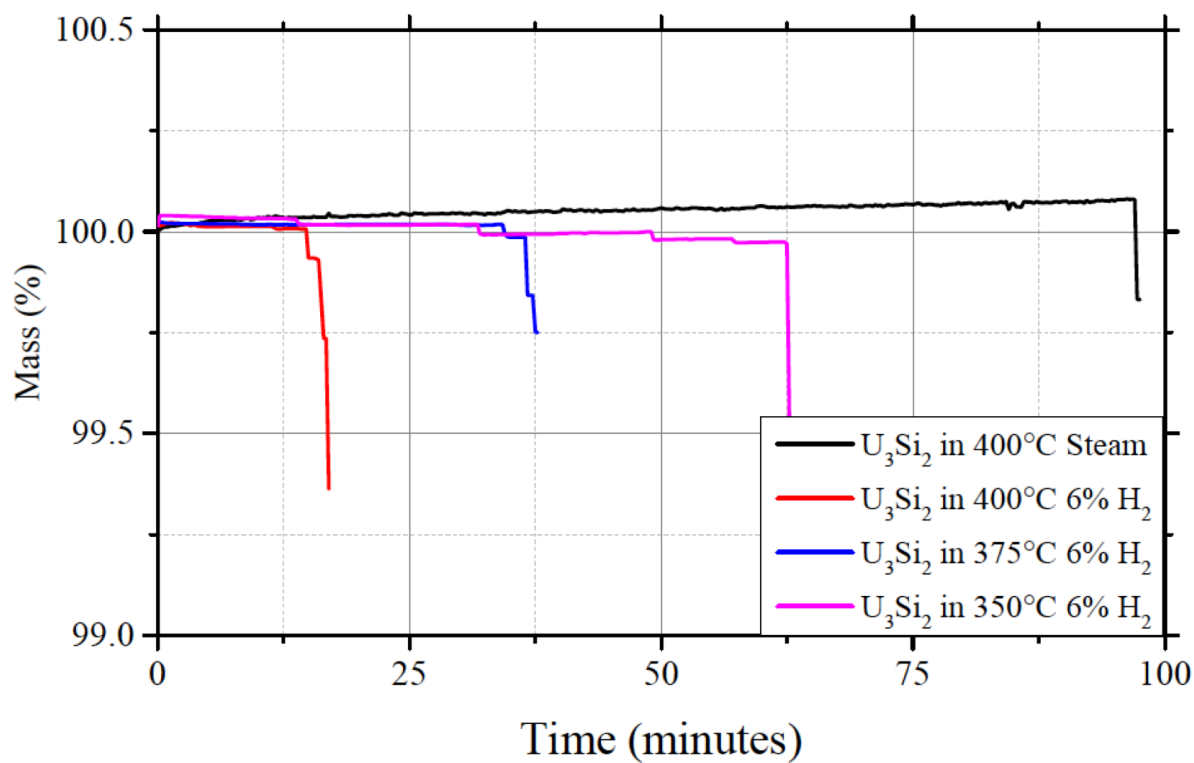


Figure 1: Isothermal exposures of  $\text{U}_3\text{Si}_2$  pellets to flowing 6%  $\text{H}_2/\text{Ar}$  at 350 (magenta), 375 (blue), and 400 (red) °C. Isothermal data for  $\text{U}_3\text{Si}_2$  in flowing steam at 400 °C is shown in black for comparison. Figure and caption adapted from (Wood et al., 2018).

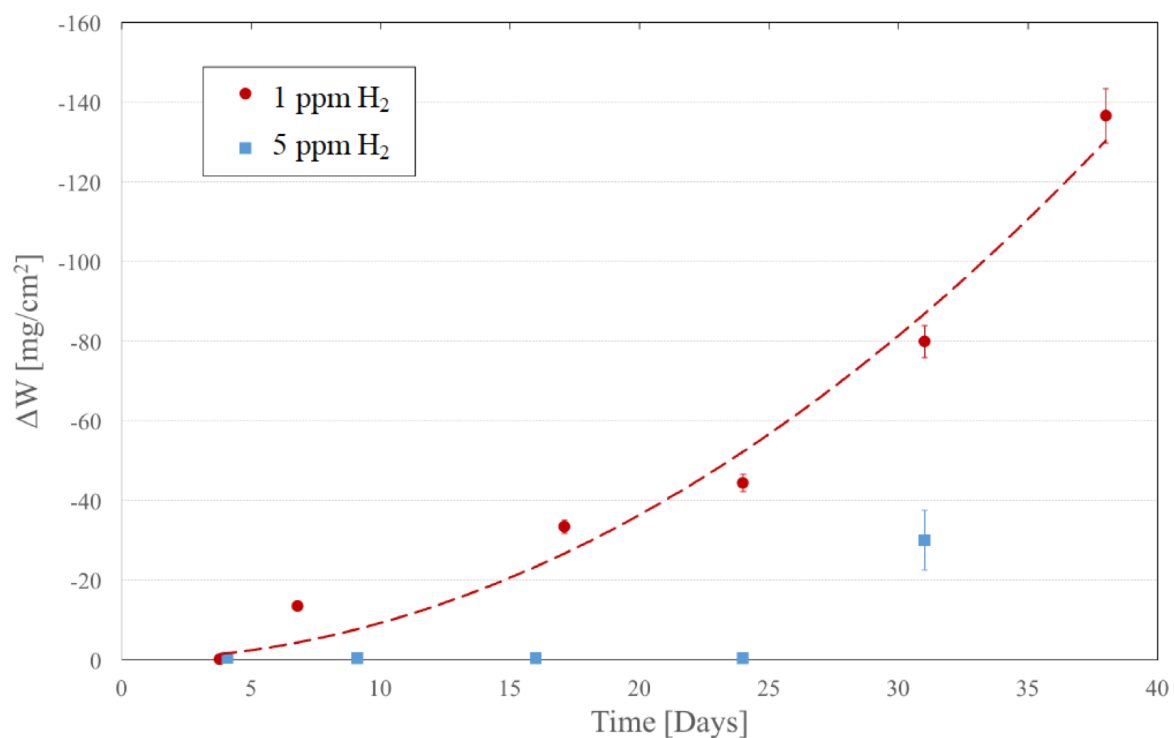


Figure 2: Weight change measured for  $U_3Si_2$  samples as a function of exposure time at 300 °C for two different water chemistry conditions. Error bars represent average of multiple samples and standard error of measurement technique. A trend line is added to the 1-ppm  $H_2$  sample data to guide the eye. Samples tested at 6-ppm  $H_2$  fully pulverized when examined after 38 days so measurement was not possible. Figure and caption adapted from (Nelson et al., 2018).



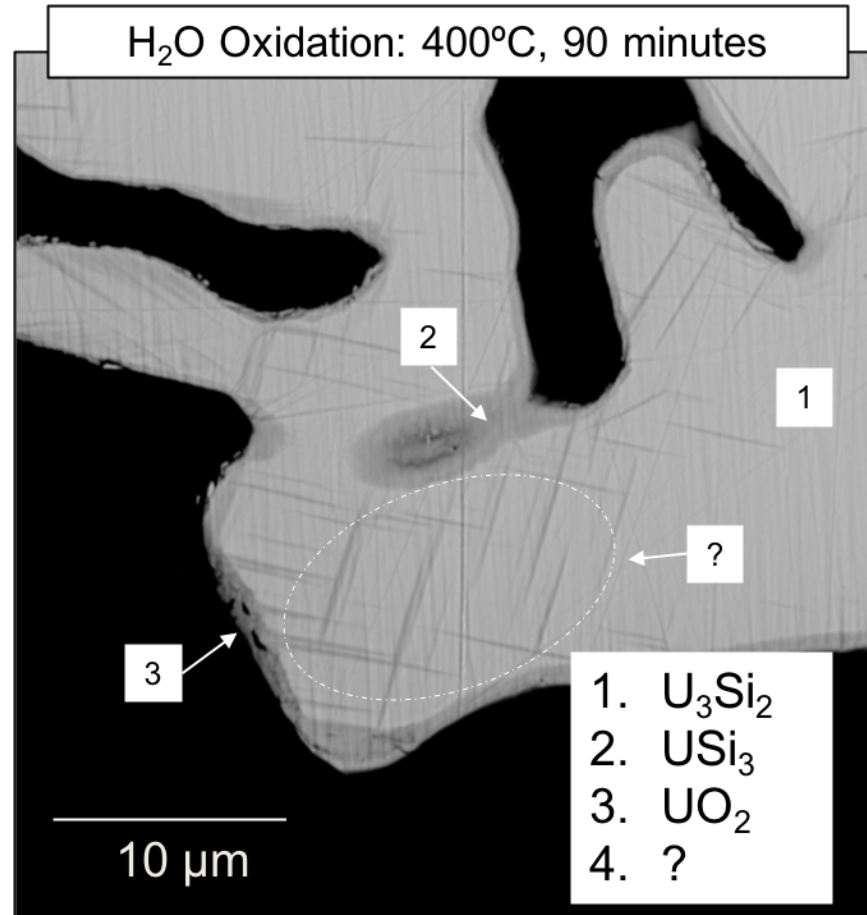


Figure 3: Micrograph taken from a cross-sectioned U<sub>3</sub>Si<sub>2</sub> pellet exposed to steam at 400 °C. Pellet was exposed for 1.5-hr. Unknown phase is hypothesized to be hydride-phase lamellae. Figure and caption adapted from (Wood et al., 2018).

This work represents a continuation of work previously performed at LANL with the specific focus on the hydriding aspects of U<sub>3</sub>Si<sub>2</sub>. In this study, a two-pronged approach to understanding U<sub>3</sub>Si<sub>2</sub> hydriding was taken: steam oxidation tests were conducted on U<sub>3</sub>Si<sub>2</sub> pellets of well-defined geometry to determine whether the onset of hydriding from a temperature standpoint could be measured while hydrogen absorption experiments using a Sieverts' apparatus were conducted on U<sub>3</sub>Si<sub>2</sub> pellets and button fragments to measure the maximum amount of hydrogen that can be absorbed by U<sub>3</sub>Si<sub>2</sub> and the hydrogen pressures required to form the hydride phase. X-ray diffraction (XRD) was also used in an attempt to understand the structure of the hydride phase.

## 2. Experimental methods

### 2.1 Materials

Buttons of  $U_3Si_2$  were synthesized by arc-melting the pure elements together in an inert, argon glovebox with oxygen and water contamination levels maintained below 0.1 ppm. Uranium metal was obtained from AeroJet Rocketdyne (Jonesborough, TN), while silicon chips were obtained from Cerac, Inc. (now Materion). Masses of uranium and silicon were measured out to match the 3:2 mole ratio in  $U_3Si_2$ .

Powder processing of  $U_3Si_2$  was performed in a high-purity argon glovebox line to minimize oxidation of powders. Phase-pure buttons, as confirmed via XRD, were crushed using a high-energy ball mill (SPEX) with 0.25 wt. % ethylene bis(stearamide) (EBS) binder for 30 minutes and subsequently sieved through a - 325 mesh sieve (44  $\mu m$ ). Pellets of  $U_3Si_2$  were pressed at 150 MPa using a 5.2-mm punch and die set so as to form approximately 5-mm OD  $\times$  2-mm thickness pellets post-sintering. These green bodies were then sintered at 1460  $^{\circ}C$  for 12-hours in gettered argon in a W-mesh furnace. Sintered pellet densities were measured using geometric methods and pellets were found to be between 81 - 87% of the theoretical density of  $U_3Si_2$ . Because dimensions were measured for density calculations, these values are considered to be conservative estimates of density. However, for this set of corrosion and gas-absorption experiments, kinetics were not of importance, so well-characterized surface areas were not necessary and lower densities were preferred to yield faster reaction rates.

### 2.2 Steam corrosion testing

A simultaneous thermal analyzer (STA 449 F3, Netzsch Instruments, Selb, Germany) with a water vapor furnace and water vapor generator (DV2ML, Astream, Germany) was used to perform steam corrosion tests of  $U_3Si_2$  pellets and measure mass change as a function of exposure time *in situ* at various temperatures. Pellets were placed in an alumina crucible to contain pulverized pellets during exposure and sample temperature was monitored using a type-S thermocouple. An image of the steam corrosion setup is shown in Figure 4.

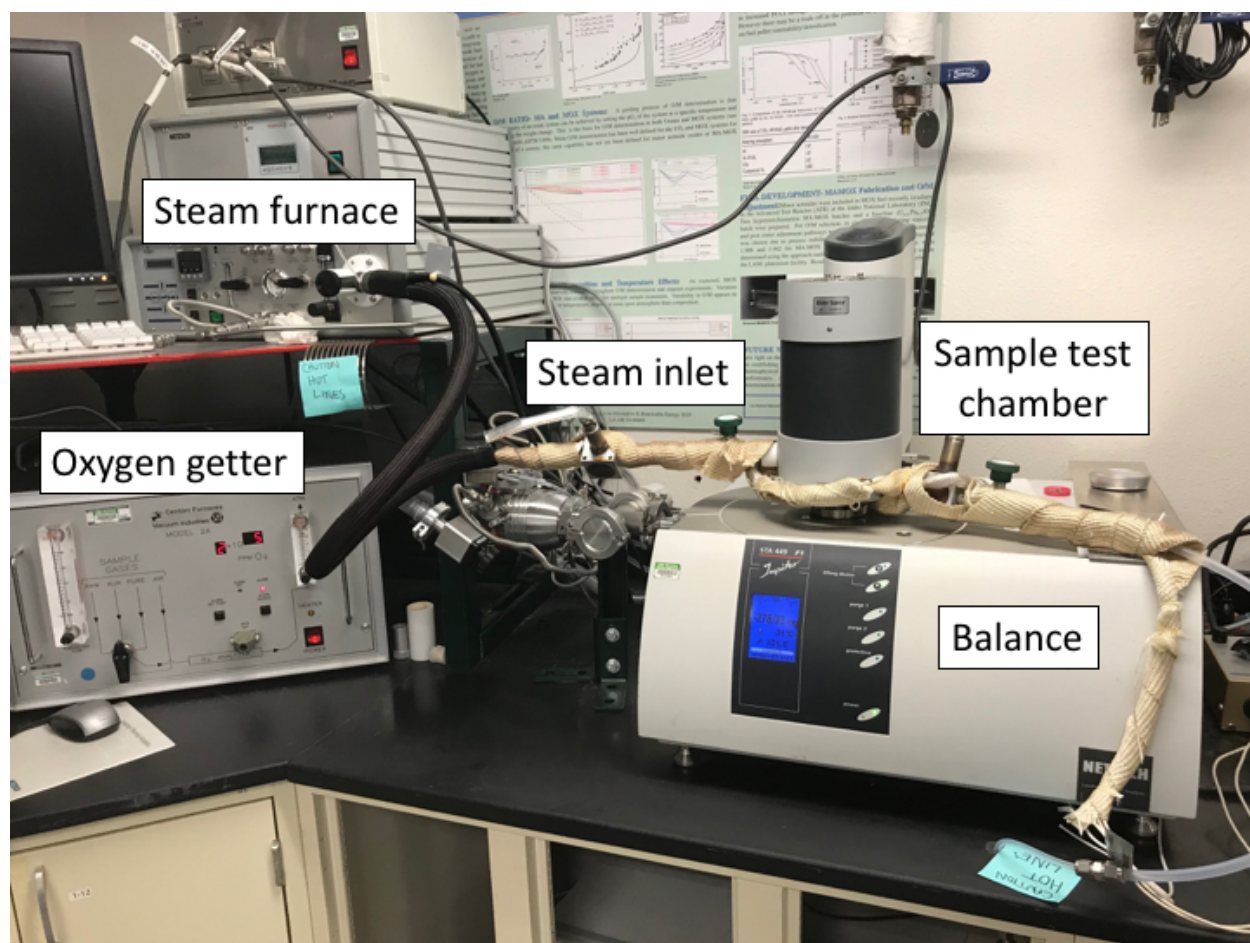


Figure 4: Experimental setup for steam TGA analysis. Annotations indicate major components of the system.

Samples were ramped up to testing temperatures in gettered argon at 10 °C/min and allowed to stabilize at the test conditions for 30-min before introduction of steam. For all tests, the water vapor flowrate was varied to maintain a consistent steam fraction of the gas depending on the testing temperature. Gettered argon at 8 L/hr (calibrated with nitrogen) acted as a carrier gas for the steam, while a protective gas of gettered argon at 20 mL/min was purged through the balance during each run. Samples were held at temperature under steam conditions for 10-hr.

## 2.3 Sieverts' gas absorption

$\text{U}_3\text{Si}_2$  pellets and button fragments were loaded in a stainless-steel reaction vessel inside an inert glovebox. The reaction vessel was attached to a gas manifold and then placed inside a tube furnace to maintain temperature. All manifold connections were composed of Swagelok VCR fitting using silver-plated nickel gaskets to provide a leak-tight seal. The whole system was evacuated and then the reaction chamber was brought to temperature. System pressure was measured using a Heise ATS 2000 0-200 psia pressure transducer, which measures absolute pressure, rather than gauge pressure. An annotated image of the Sieverts' apparatus is shown in Figure 5.

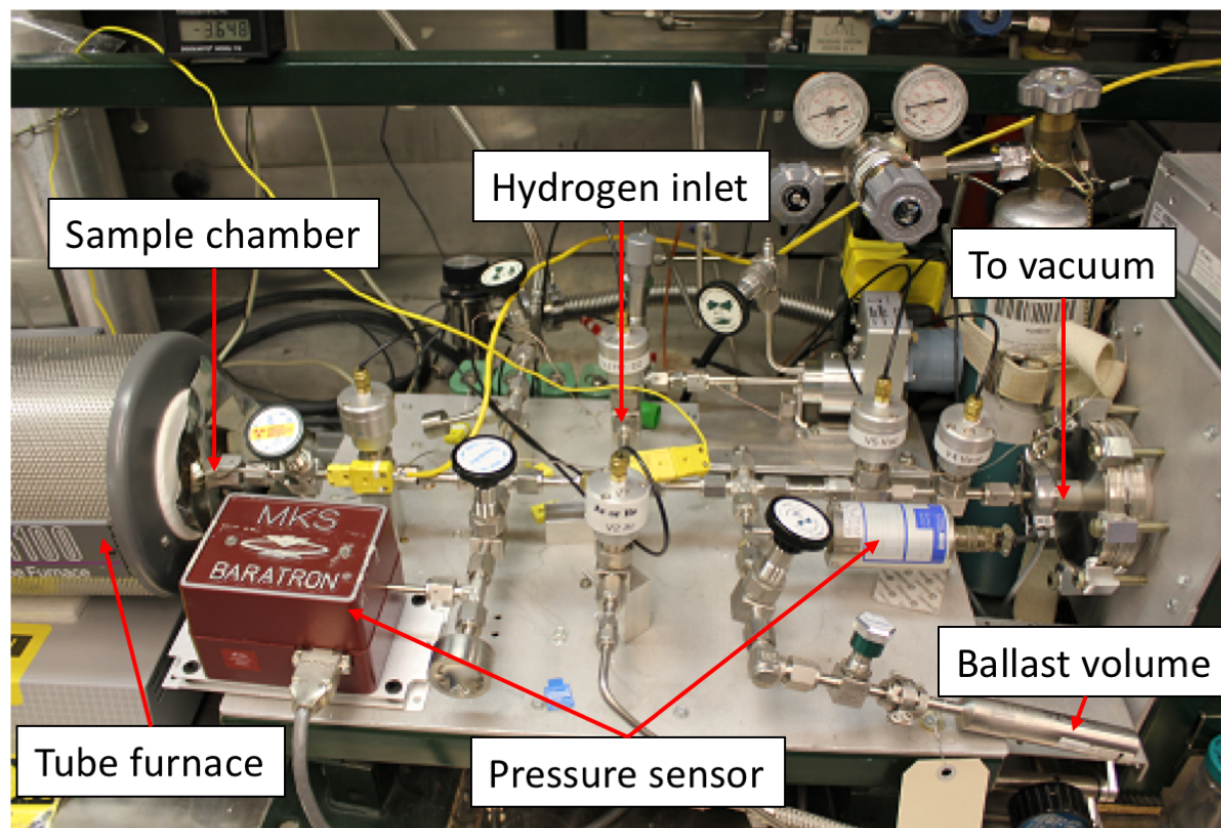


Figure 5: Experimental apparatus for Sieverts' gas absorption. Important components of the apparatus are annotated.

Volume calibration was performed using a 52.67-mL calibrated expansion volume. The calibrated volume was filled with a known pressure of helium gas and then opened to the manifold and the sample reaction chamber. The manifold and reaction chamber volumes were then calculated using Boyle's Law ( $P_1V_1 = P_2V_2$ ). This process was performed four times to calculate average values for the relevant volumes.

Hydrogen dosing was performed by injecting a known pressure of hydrogen. Once the pressure had equilibrated within the manifold, the valve to the reaction chamber was opened and the gas allowed to equilibrate in the reaction chamber. Equilibration in the reaction chamber was due to gas expansion into the increased volume and absorption of hydrogen by the sample. The gas pressure was allowed to equilibrate for one hour, after which the sample chamber was isolated from the manifold and gas was aliquoted again and the process repeated. Measurements were terminated once the system reached a pressure value that was pre-defined in the experiment definition. Hydrogen aliquoting was controlled using a LabView program based off readings from the Heise pressure transducer.

Moles of gas absorbed were calculated from the ideal gas law using aliquot pressures and volumes and reaction equilibrium pressures and volumes. These were then compared with the initial moles of uranium in  $U_3Si_2$  to calculate the hydrogen-to-uranium (H/U) ratio. After testing, samples were sealed in the reaction vessel and transferred to sample storage vials in an inert glovebox with oxygen levels maintained below 1-ppm to minimize degradation of the hydrided  $U_3Si_2$ .

## 2.4 Microstructural analysis

XRD was used to confirm the composition of the initial  $U_3Si_2$  buttons and to also analyze the hydrided  $U_3Si_2$ . A Bruker XRD (D2 Phaser, Bruker AXS, Madison, WI, USA) was used for these analyses.



Compositional analyses of buttons were performed with quick XRD scans with  $2\theta$  ranging between 10 and  $90^\circ$  with a  $0.02^\circ$   $2\theta$  step and a 2-s acquisition time for each step. Hydride phase analysis was performed using longer scans with the same  $2\theta$  range but a  $2\theta$  step size of  $0.01^\circ$  and 5-s acquisition time. Material for all XRD examinations were homogenized using a mortar and pestle in an inert, argon glovebox and encapsulated in a low-background XRD sample holder to prevent exposure to air.

### 3. Results and discussion

#### 3.1 Steam corrosion testing

As mentioned earlier, pellets of  $U_3Si_2$  were exposed to steam at various temperatures to determine the onset of hydriding. To do this, mass change was measured as a function of exposure time and degradation mechanism was noted (i.e. ejection of pellet fragments vs. pulverization). Mass change (in percent) as a function of exposure time for each testing temperature is shown in Figures 6 - 9. Testing temperatures were  $250^\circ\text{C}$  (Figure 6),  $300^\circ\text{C}$  (Figure 7),  $350^\circ\text{C}$  (Figure 8), and  $500^\circ\text{C}$  (Figure 9). Inset in each of these figures is the physical appearance of the sample after testing. It should be noted that large spikes in mass change in these figures are an artifact of the steam generator, rather than physical mass changes.

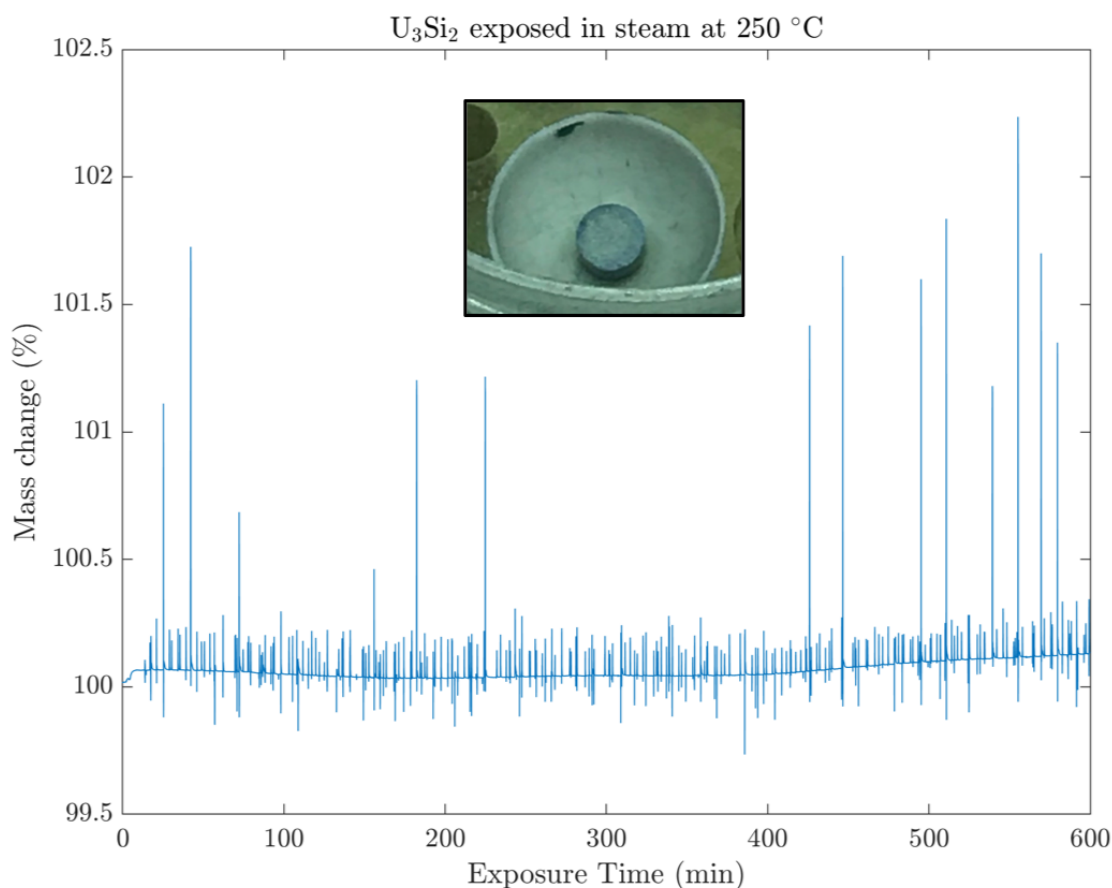


Figure 6: Mass gain for  $U_3Si_2$  exposed to 75% steam at  $250^\circ\text{C}$  for 10-hr. Data is smoothed using a moving average filter with moving average span of 5. In the inset is an image of the sample post-testing.

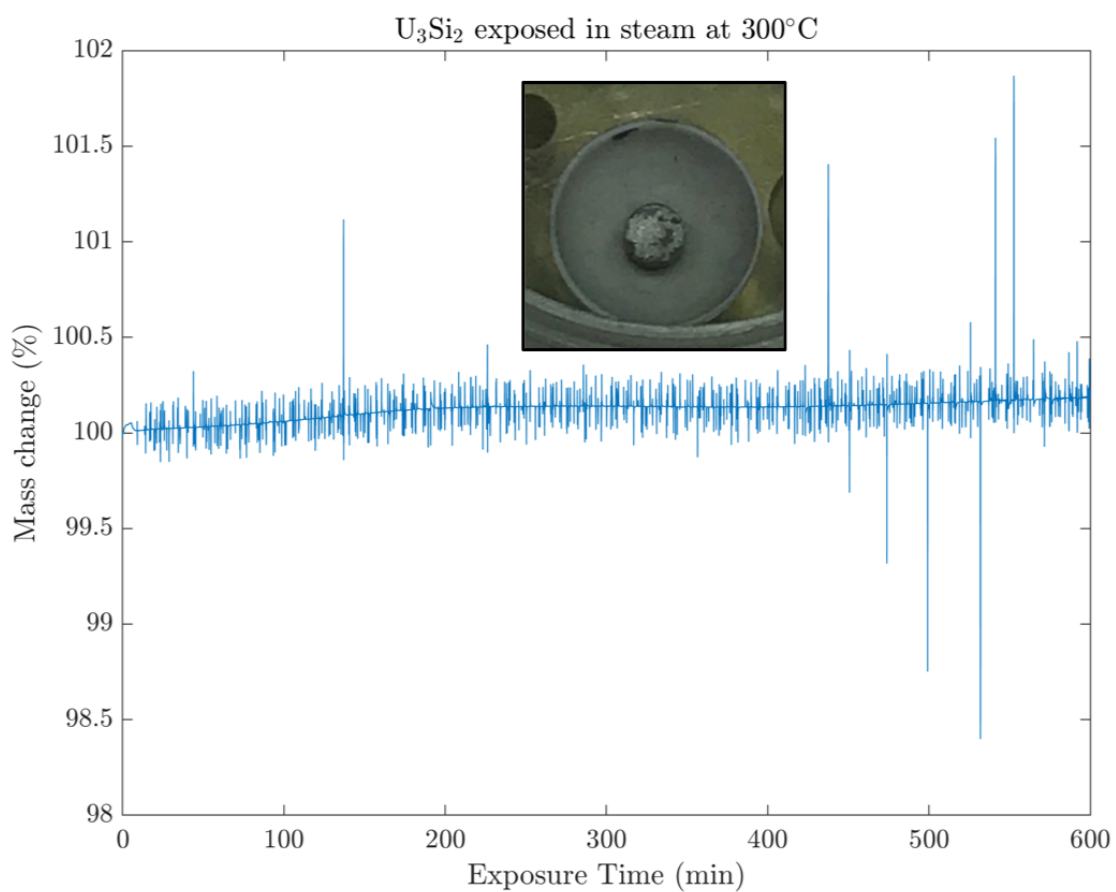


Figure 7: Mass gain for  $\text{U}_3\text{Si}_2$  exposed to 75% steam at 300 °C for 10-hr. Data is smoothed using a moving average filter with moving average span of 5. In the inset is an image of the sample post-testing.

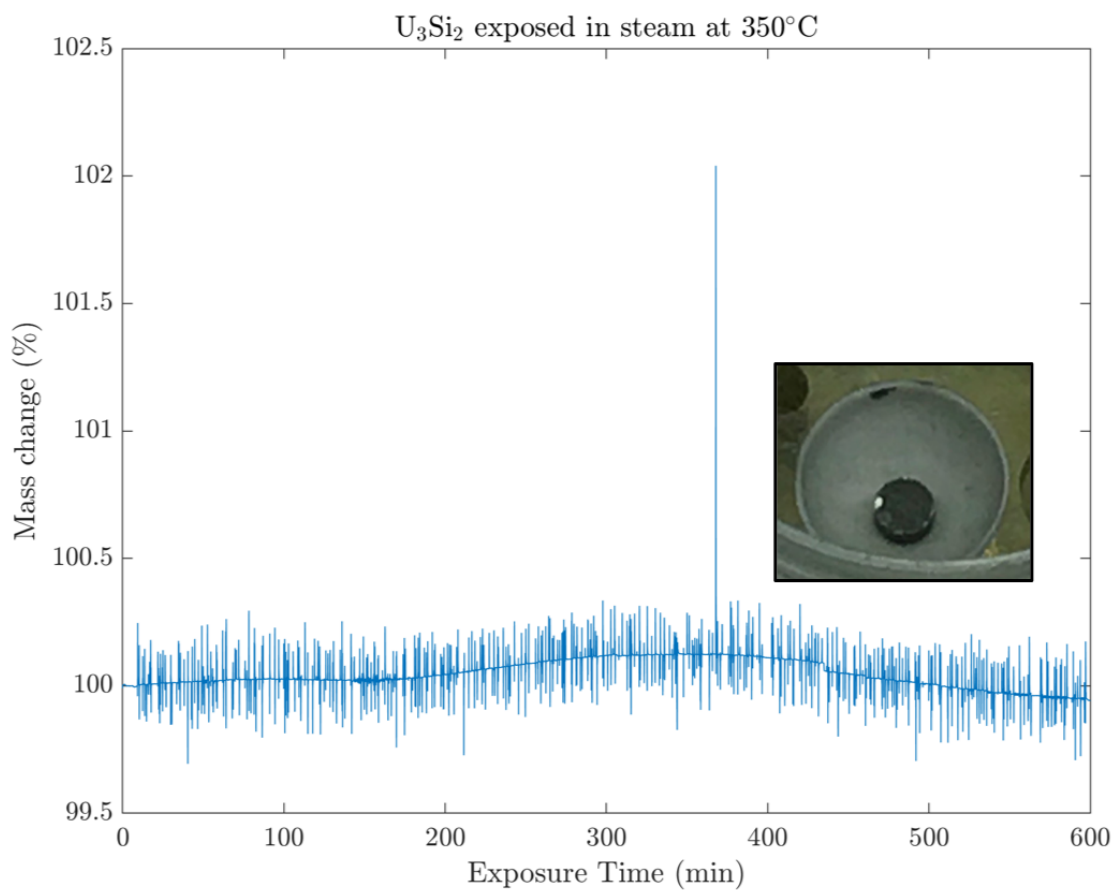


Figure 8: Mass gain for  $\text{U}_3\text{Si}_2$  exposed to 75% steam at 350 °C for 10-hr. Data is smoothed using a moving average filter with moving average span of 5. In the inset is an image of the sample post-testing.

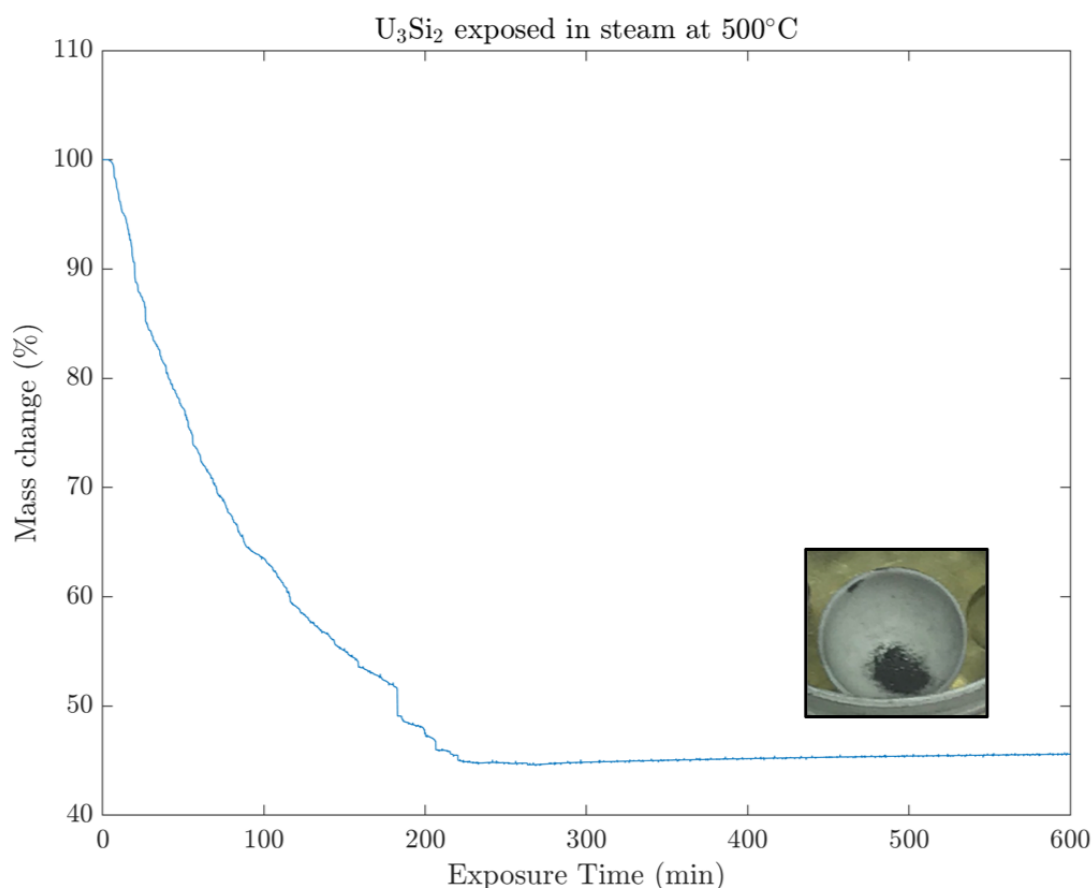


Figure 9: Mass gain for  $\text{U}_3\text{Si}_2$  exposed to 75% steam at 500 °C for 10-hr. Data is smoothed using a moving average filter with moving average span of 5. In the inset is an image of what remained of the sample post-testing.

Figure 6 shows that, in 75% steam at 250 °C,  $\text{U}_3\text{Si}_2$  did not seem to change appearance with exposure time and mass change was minimal, though a slight color change was noted. Very small mass changes were also observed for steam testing at 300 (Figure 7) and 350 (Figure 8) °C, though the inset images show the slow development of oxide on the surface, with the surface of the sample tested at 350 °C almost fully covered by an oxide layer. Figure 9 shows the mass change as a function of exposure time for  $\text{U}_3\text{Si}_2$  in 75% steam at 500 °C. For this test, mass was observed to consistently decrease as a function of time. This was not due to actual mass change of the sample, but rather ejection of pellet fragments during oxidation testing. The end result of this test was an inactive, black powder (shown in the inset of Figure 9), which is consistent with observations in previous work and measurement of  $\text{U}_3\text{O}_8$ . Another test performed at 700 °C exhibited rapid mass loss in the absence of steam and a large temperature increase upon addition of steam (large enough to soft-reset the instrument). The sample condition after testing is shown in Figure 10, which indicates partial oxidation of the pellet and spalled oxide.

Comparison of mass changes for the low-temperature tests (250, 300, and 350 °C) is shown in Figure 11. Data is severely smoothed and is only used to compare general trends in mass change. This comparison shows that, at both 250 and 300 °C,  $\text{U}_3\text{Si}_2$  appeared to gain a very small amount of mass, though it is not clear whether this was from oxidation, hydrogen absorption, or an artifact of the technique due to baseline drift. Previous work on  $\text{U}_3\text{Si}_2$  in steam at similar temperatures resulted in samples described as having no mass change or structural degradation, so it is still unclear what the cause of the measured mass changes might be. While the sample exposed at 250 °C exhibited no clear oxide scale, the surface of the sample



exposed at 300 °C displayed small patches of oxide, which is consistent with measured mass gain in Figure 11. Beyond approximately 400 minutes, mass change for  $\text{U}_3\text{Si}_2$  exposed at 350 °C shows a very slight mass decrease. Because of the presence of black-colored powder on the instrument fixturing after the corrosion test, it is hypothesized that 350 °C is near the temperature where  $\text{U}_3\text{Si}_2$  begins to degrade and fall apart in steam. Figure 12 shows a comparison between all steam corrosion data sets and is primarily to highlight the extent of mass loss at high temperature due to ejection of sample fragments during testing.



Figure 10:  $\text{U}_3\text{Si}_2$  exposed to 75% steam at 700 °C. Corrosion test lasted only a few seconds before the temperature spike due to oxidation caused a soft reset of the instrument.

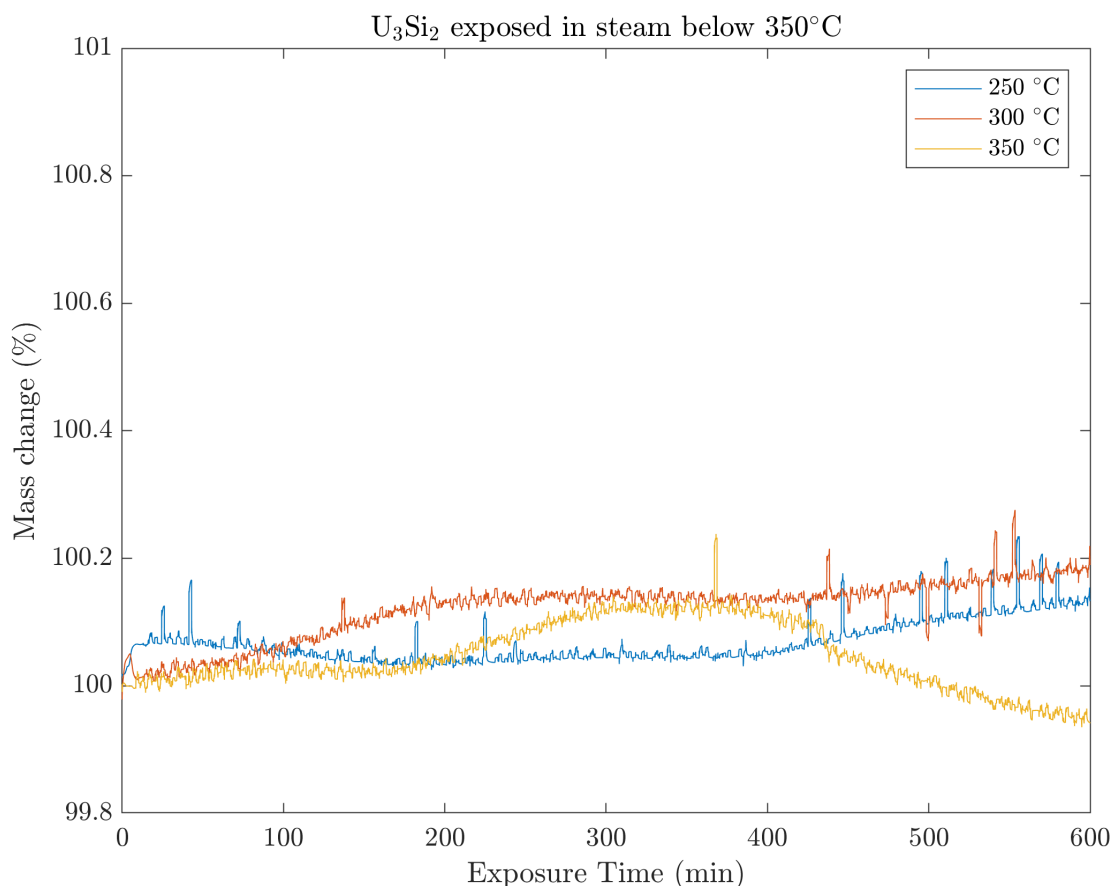


Figure 11: Comparison between mass gains at 250 (blue), 300 (orange), 350 (yellow) °C in 75% steam. Data is smoothed to show general trends in mass change, only, and is not considered analytical.

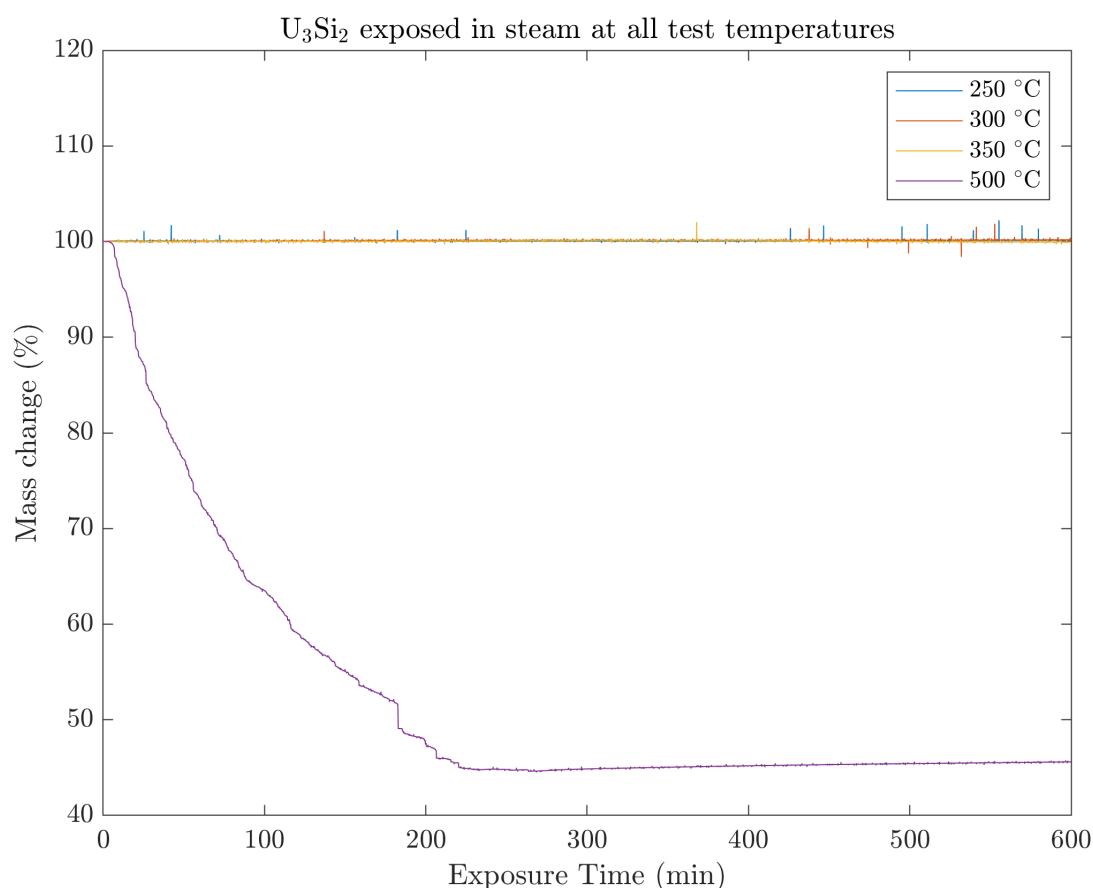


Figure 12: Comparison between mass gains at 250 (blue), 300 (orange), 350 (yellow), and 500 (purple) °C in 75% steam. Data is smoothed using a moving average filter with moving average span of 5.

In FY17 work, it was hypothesized that the hydriding could be separated from oxidation by determining the limits of stability for the  $\text{U}_3\text{Si}_2$  hydride during steam oxidation tests. From these results, it is clear that, using thermogravimetry alone, it is not possible to determine the regimes of stability for  $\text{U}_3\text{Si}_2$  hydriding versus oxidation in steam. At low temperatures,  $\text{U}_3\text{Si}_2$  was not observed to change mass significantly, whereas, at high temperatures, the oxidation reaction occurred so rapidly that it was difficult to determine whether oxidation or hydriding were the dominant degradation mechanisms. Hydriding could not be fully ruled out because mass changes due to absorption of hydrogen are small: fully hydriding  $\text{U}_3\text{Si}_2$  to  $\text{UH}_3$  will result in a mass change of approximately 1.2% and decoupling this from mass change due to oxidation is very difficult. Based on the difficulty of such an analysis, it was concluded that steam oxidation testing of  $\text{U}_3\text{Si}_2$  at elevated temperatures would not aid in assessing hydriding and corrosion performance.

## 3.2 Sieverts' gas absorption

For hydrogen absorption experiments, samples of  $\text{U}_3\text{Si}_2$ , both pellets and button fragments, were placed in a stainless-steel reaction chamber, which was connected to a gas manifold and then placed inside a tube furnace to maintain testing temperature. Hydrogen was added to a known pressure in the manifold with a known volume. From this the initial moles of hydrogen were calculated using the ideal gas law. The sample chamber was opened to the manifold, allowing the gas to flow into the sample chamber. The pressure was allowed to equilibrate for one hour and then measured. From this, the final number of hydrogen moles in the gas phase was determined. Using both initial and final moles of hydrogen, the amount of hydrogen

absorbed by the sample was able to be calculated and then converted to a hydrogen-to-uranium atomic ratio based on the initial mass of uranium in the  $\text{U}_3\text{Si}_2$  sample.

From these data, a pressure-composition isotherm for  $\text{U}_3\text{Si}_2$  was able to be calculated for each temperature, as shown in Figure 13 at 350 °C, which plots equilibrium pressure of hydrogen as a function of the hydrogen-to-uranium ratio.

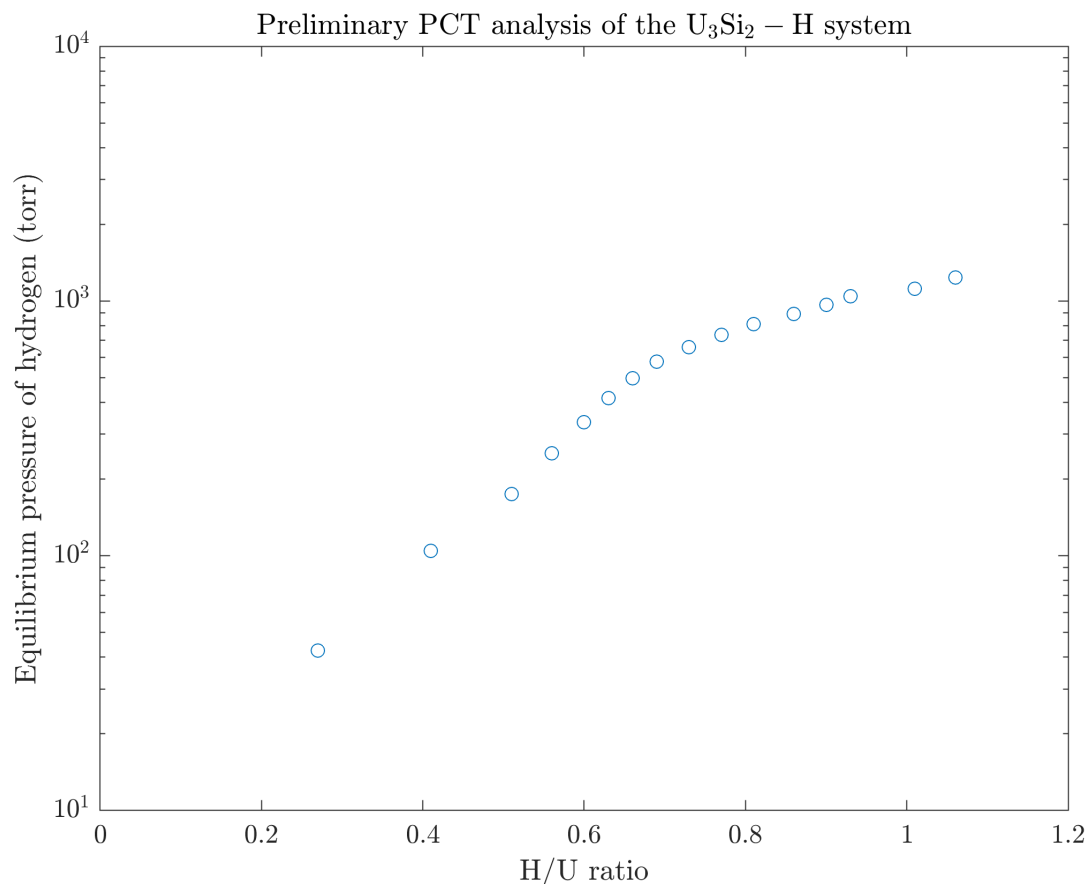


Figure 13: Preliminary pressure-composition-isotherm for  $\text{U}_3\text{Si}_2$  in hydrogen at 350 °C. Final H/U ratio was calculated to be 1.06.

Preliminary data studying the  $\text{U}_3\text{Si}_2 - \text{H}$  system at 350 °C is plotted in Figure 13. In this plot, the initial, sloped rise in hydrogen pressure is attributed to accommodation of hydrogen in the  $\text{U}_3\text{Si}_2$  lattice as solid-solution atoms. After the initial increase in hydrogen pressure, there is typically a plateau region where aliquoting more hydrogen would result in the same pressure of hydrogen; such a plateau region would indicate the transformation of  $\text{U}_3\text{Si}_2$  with hydrogen in solid-solution to a true hydride phase. The pressure-composition isotherm in Figure 13 for 350 °C does not exhibit a true plateau region, which implies that increasing hydrogen pressures are needed to drive further hydrogen absorption in  $\text{U}_3\text{Si}_2$ . This particular sample was exposed to hydrogen up to a calculated H/U ratio of 1.06.

The pressure of hydrogen required to hydride  $\text{U}_3\text{Si}_2$  (up to 1200 torr in Figure 13) is much higher than those required to hydride pure uranium (350 torr at 350 °C). Two possible explanations for this are that (1) the silicon in  $\text{U}_3\text{Si}_2$  presents a barrier to hydrogen absorption and that, upon hydriding,  $\text{U}_3\text{Si}_2$  separates to  $\text{UH}_3$  and Si or (2)  $\text{U}_3\text{Si}_2$  hydrides to a separate phase,  $\text{U}_3\text{Si}_2\text{H}_x$ , as has been proposed in literature.

Microstructural analysis of  $U_3Si_2$  hydrided to termination has yet to be done, but would provide evidence for either explanation.

### 3.3 Microstructural analysis

XRD was performed on  $U_3Si_2$  exposed to hydrogen at 860 torr and 400 °C. Results were compared with the Powder Diffraction File (PDF) for  $U_3Si_2$ , as well as XRD data from previous work on  $U_3Si_2$  exposed in 6%  $H_2$ /Ar for 50-hr and literature data of  $U_3Si_2H_{1.8}$ . This comparison is plotted in Figure 14.

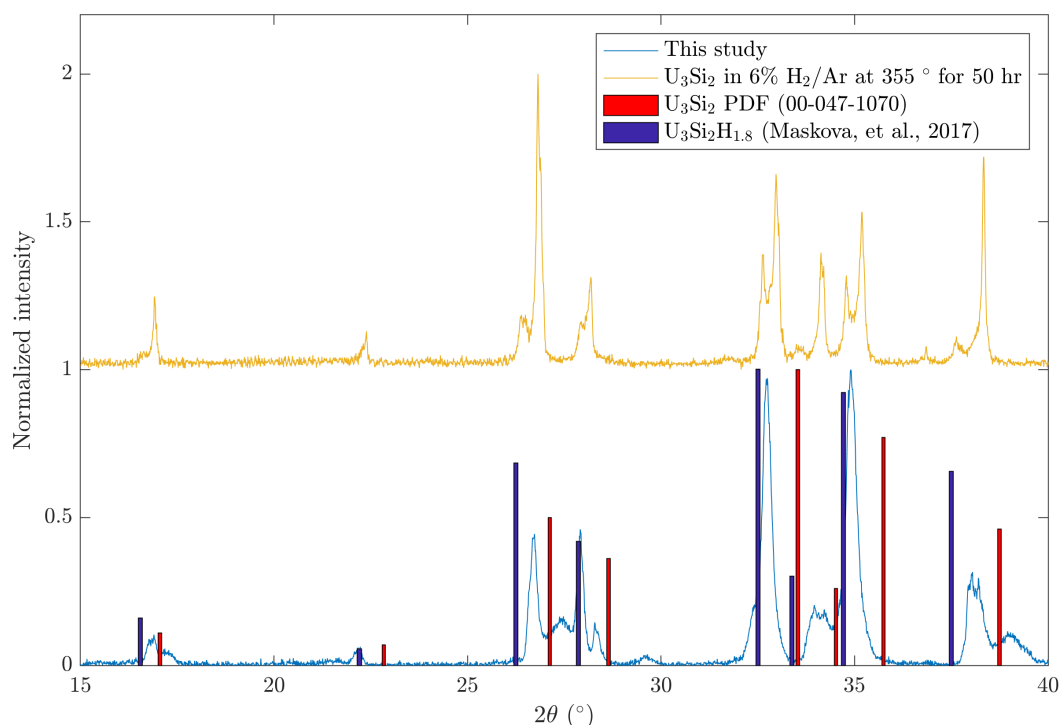


Figure 14: XRD pattern collected from  $U_3Si_2$  exposed to hydrogen gas at 860 torr and 400 °C. Data from this study is shown in blue, while data from exposure of  $U_3Si_2$  to flowing 6%  $H_2$ /Ar at 355 °C for 50-hr from (Wood et al., 2018). Red bars indicate the PDF peak indices for  $U_3Si_2$ , while blue bars indicate peak indices for  $U_3Si_2H_{1.8}$  from (Mašková et al., 2017, p. 2).

The results from this work are shown in blue lines, while the results from exposure in 6%  $H_2$ /Ar are shown in yellow (offset). Red bars represent peak indices from the PDF for  $U_3Si_2$ , while blue bars represent peak indices for  $U_3Si_2H_{1.8}$  from literature (Mašková et al., 2017, p. 2). Figure 14 shows that the peaks associated with  $U_3Si_2$  hydrided at 400 °C are shifted to lower  $2\theta$  than for pure  $U_3Si_2$ , but higher  $2\theta$  than for  $U_3Si_2H_{1.8}$ . Because the diffraction peaks are simply shifted to lower  $2\theta$  as compared with the PDF for  $U_3Si_2$ , it is hypothesized that all of the hydrogen in the sample was entirely in solid-solution. This would result in an expansion of the  $U_3Si_2$  lattice and, thus, a shift in XRD pattern peak position to lower  $2\theta$  (higher d-spacing). This is in contrast with the diffraction pattern, taken from (Wood et al., 2018), for  $U_3Si_2$  in 6%  $H_2$ /Ar, which has shoulder peaks at the indices for  $U_3Si_2H_{1.8}$  and larger peaks at the indices for  $U_3Si_2$ , which could indicate phase separation in the sample. Hydrogen absorption to termination of hydriding should be performed and the sample analyzed via XRD for confirmation of the  $U_3Si_2H_{1.8}$  structure.

## 4. Summary and future work

Steam corrosion and hydriding performance of  $U_3Si_2$  were studied using steam-coupled thermogravimetry and Sieverts' gas absorption, respectively. Steam oxidation results showed that  $U_3Si_2$

does not appreciably degrade below 350 °C and that, above this temperature, rapid ejection of sample fragments occurs. It was determined that it was difficult to decouple hydriding from oxidation due to the rapidity of oxidation and fragment ejection. Hydrogen absorption results showed that  $\text{U}_3\text{Si}_2$  requires much higher pressures of hydrogen to absorb it than does pure uranium metal.  $\text{U}_3\text{Si}_2$  was hydrided to H/U ratios of 1.06 at 350 °C, though hydriding was not performed to termination. Preliminary results suggest that this would require hydrogen pressures much higher than what was achieved in this study.

Future experiments studying hydriding of  $\text{U}_3\text{Si}_2$  will focus on higher pressures of hydrogen to drive the hydrogen absorption reaction to termination, when the hydrogen pressure will rapidly increase with little absorption of hydrogen. This will be further expanded by studying hydriding at higher temperatures and attempt to understand conditions where  $\text{U}_3\text{Si}_2$  hydriding might be unfavorable during cladding-breach conditions based on gas absorption experiments. Analysis of the plateau pressures for hydriding will also enable the calculation of the formation enthalpy and entropy of the hydride, as well as formation enthalpies for various  $\text{U}_3\text{Si}_2 - \text{H}$  compounds, which will provide fundamental thermodynamic properties of this newly-identified phase. Future work will focus on coupling Sieverts' gas absorption-type experiments with thermogravimetric analysis to determine degradation mechanisms of prospective LWR fuels.

## 5. Bibliography

- Mašková, S., Miliyanchuk, K., Havela, L., 2017. Hydrogen absorption in  $U_3Si_2$  and its impact on electronic properties. *J. Nucl. Mater.* 487, 418–423. <https://doi.org/10.1016/j.jnucmat.2017.02.036>
- Middleburgh, S.C., Claisse, A., Andersson, D.A., Grimes, R.W., Olsson, P., Mašková, S., 2018. Solution of hydrogen in accident tolerant fuel candidate material:  $U_3Si_2$ . *J. Nucl. Mater.* 501, 234–237. <https://doi.org/10.1016/j.jnucmat.2018.01.018>
- Nelson, A.T., Migdisov, A., Wood, E.S., Grote, C.J., 2018.  $U_3Si_2$  behavior in  $H_2O$  environments: Part II, pressurized water with controlled redox chemistry. *J. Nucl. Mater.* 500, 81–91. <https://doi.org/10.1016/j.jnucmat.2017.12.026>
- Wood, E.S., White, J.T., Grote, C.J., Nelson, A.T., 2018.  $U_3Si_2$  behavior in  $H_2O$ : Part I, flowing steam and the effect of hydrogen. *J. Nucl. Mater.* 501, 404–412. <https://doi.org/10.1016/j.jnucmat.2018.01.002>